



www.chemasianj.org

Sunlight Powered Continuous Flow Reverse Water Gas Shift Process Using a Plasmonic Au/TiO₂ Nanocatalyst

Pau Martínez Molina,^[a] Koen W. Bossers,^[a] Jelle D. Wienk,^[a] Jelle Rohlfs,^[a] Nicole Meulendijks,^[a] Marcel A. Verheijen,^[b, c] Pascal Buskens,^{*[a, d]} and Francesc Sastre^{*[a]}

Abstract: The continuous flow reverse water gas shift (rWGS) process was efficiently catalyzed by a plasmonic Au/TiO_2 nanocatalyst using sunlight as sole and sustainable energy source. The influence of the catalyst bed thickness on the CO production rate was studied, and three different catalytic regimes were identified as direct plasmon catalysis (DPC), shielded plasmon catalysis (SPC) and unused plasmon catalysis (UPC). The CO_2 : H_2 ratio was optimized to 4:1 and a maximum CO production rate of 7420 mmol·m $^{-2} \cdot h^{-1}$ was

achieved under mild reaction conditions (p=3.5 bar, no external heating, $E_e=14.0~{\rm kW\cdot m^{-2}}$), corresponding to an aparent quantum efficiency of 4.15%. The stability of the Au/TiO₂ catalyst was studied for 110 h continuous operation, maintaining more than 82% of the initial CO production rate. On/off experiments mimicking discontinuous sunlight powered processing furthermore showed that the Au/TiO₂ catalyst was stable for 8 consecutive runs.

Introduction

CO₂ capture and utilization (CCU) technologies are expected to play an important role in the near future to produce platform chemicals, polymers, and synthetic fuels to power e.g. heavy transport and aviation.[1] Technically scalable and economically feasible CCU concepts are required to achieve a fully defossilized carbon economy. In the past decades, several CO₂ conversion technologies have been explored, such as biocatalytic, electrochemical, photo(electro)chemical and thermochemical processes. [1-2] Photochemical processes are attractive because of their potential for direct use of sunlight as sustainable energy source and their typical clean production under mild reaction conditions.[3] To achieve efficient sunlight utilization and high production rates, plasmonic metal nanoparticles (NPs) have been applied as catalysts, in specific cases in combination with a semiconductor. [4] Plasmonic NPs can efficiently harvest sunlight because of their localized surface plasmon resonance (LSPR).^[5] The light frequency at which a metallic NP experiences its LSPR depends amongst others on the nature of the metal, size and shape of the NP and the distance between NPs. [6] Furthermore, supported metallic NPs can serve as catalysts, offering a large number of active sites on their chemically reactive surface.

CO₂ can be reduced to chemicals and fuels via catalytic hydrogenation, leading to products such as CH₄ and CO.^[7] CH₄ is produced in the Sabatier reaction (Eq. 1), whilst CO is obtained by the reverse water gas shift (rWGS) process (Eq. 2). Syngas, a mixture of CO and H₂, can be applied to produce methanol, and long chain hydrocarbons using Fischer-Tropsch synthesis.^[8] Therefore, the rWGS reaction can serve as first step for the production of synthetic fuels and chemicals from CO₂.

$$CO_2 + 4H_2 \rightarrow CH_4 + 2H_2O \Delta H_{298K} = -165.0 \text{ kJ} \cdot \text{mol}^{-1}$$
 (1)

$$CO_2 + H_2 \rightleftharpoons CO + H_2O \qquad \Delta H_{298K} = 41.2 \text{ kJ} \cdot \text{mol}^{-1}$$
 (2)

The rWGS reaction is endothermic and limited by equilibrium.^[9] In thermocatalysis temperatures above 800°C are required to produce CO with a selectivity above 80%. [10] At lower temperatures, CH₄ production is favoured. As alternative to the thermocatalytic process, plasmonic catalysis aims to use metallic NPs, to harvest the energy of (sun)light and use it to drive the reaction. When metallic nanoparticles are exposed to light, free electrons display a resonant response based on the localized surface plasmon resonance (LSPR). This coherent oscillation dephases and generates hot electrons, which can promote the rWGS reaction in three main ways: (1) they can be transferred to unoccupied molecular orbitals of reactants adsorbed on the surface of the metal nanocatalyst to induce bond dissociation (non-thermal contribution), (2) they can be injected into the conduction band of the semiconductive support and thereby enhance the photocatalytic activity of the semiconductor (non-thermal contribution), and (3) they can thermalize via electron-electron and electron-phonon scatter-

The Netherlands Organisation for Applied Scientific Research (TNO), High Tech Campus 25, 5656 AE Eindhoven (The Netherlands)

E-mail: pascal.buskens@tno.nl

francesc.sastrecalabuig@tno.nl

[b] Dr. M. A. Verheijen

Eurofins Materials Science, High Tech Campus 11, 5656 AE Eindhoven (The Netherlands)

[c] Dr. M. A. Verheijen

Department of Applied Physics, Eindhoven University of Technology, 5600 MB Eindhoven (The Netherlands)

[d] Prof. Dr. P. Buskens

Design and Synthesis of Inorganic Materials (DESINe), Institute for Materials Research, Hasselt University, Agoralaan Building D, 3590 Diepenbeek (Belaium)

Supporting information for this article is available on the WWW under https://doi.org/10.1002/asia.202300405

[[]a] P. Martínez Molina, Dr. K. W. Bossers, J. D. Wienk, J. Rohlfs, N. Meulendijks, Prof. Dr. P. Buskens, Dr. F. Sastre



ing, resulting in an increased temperature of the catalyst (photothermal contribution).

Supported noble metal nanocatalysts based on Au have been reported to reach the highest activities in the light powered rWGS reaction. Huber et al. studied the performance of Au NPs supported on different metal oxides at 400°C and visible light irradiation (5216 W·m⁻²), reporting a CO₂ conversion rate of 2663 μ mol· g_{cat}^{-1} ·min⁻¹.[11] Several catalysts based on Au and Ag NPs supported on TiO2 were studied by Tahir et al., unravelling the potential of different TiO2 morphologies and the use of bimetallic catalysts. They investigated Au/TiO₂ nanostructures, with maximum activity of 4144 μ mol·g_{cat}⁻¹·h⁻¹ under 150 mW·cm⁻² irradiance.^[12] Bobadilla et al. recently studied the role of oxygen vacancies in the rWGS reaction, and proposed a redox mechanism for Au/TiO2 catalysts with involvement of Ti³⁺ species.^[13] They suggested the formation of hydroxy carbonyl intermediates, which further decompose to CO and water. Alternative metals, such as Ag, Fe and Cu also catalyse the light-powered rWGS reaction, albeit with lower activity.[14] Other metals, such Ru and Ni have shown a strong selectivity towards CH₄ production.^[7a,d,h,15] Recently, our group has reported plasmonic Au nanoparticles supported on TiO₂ that promote the rWGS reaction under sunlight irradiation without any external heating in a batch process. [7e,f] We reported a maximum CO initial production rate of 429 mmol \cdot g_{Au}⁻¹ \cdot h⁻¹ (8525 mmol·m⁻²·h⁻¹) with a selectivity of 98% and an apparent quantum efficiency of 4.7% using mildly concentrated sunlight $(1.44 \text{ W}\cdot\text{cm}^{-2}=14.4 \text{ suns})$ in a batch process.

To scale up and progress towards an industrially applicable technology, is of vital importance (i) to transfer from a batch to a continuous flow process and (ii) to maximize the CO production rate per m⁻² illuminated catalyst bed to minimize land use. Furthermore, it is crucial to study (iii) the catalyst stability over a prolonged period of time and (iv) in on-off experiments to mimic discontinuous sunlight powered production. In this study, we address these four challenges for the sunlight powered rWGS process.

Results and discussion

Catalyst synthesis and characterization

The Au/TiO₂ catalyst was synthesized via a deposition-precipitation method reported previously and described in more detail in the experimental section and previously reported. The Au loading was analyzed through Inductively Coupled Plasma-Atomic Emission Spectroscopy (ICP-AES), yielding a Au content of 3.1 wt.%. Representative High-Angle Annular Dark Field-Scanning Transmission Electron Microscopy (HAADF-STEM) images display TiO₂ nanoparticles decorated with small Au nanospheres (Figure 1a). The average Au particle size was determined by measuring 200 NPs, resulting in an average diameter of 1.70 nm, and following a lognormal distribution (Figure 1b). The diffuse UV-visible reflectance spectra showed a large difference between the TiO₂ anatase support and the Au/TiO₂ catalyst (Figure 1c). In the first case, light absorption was

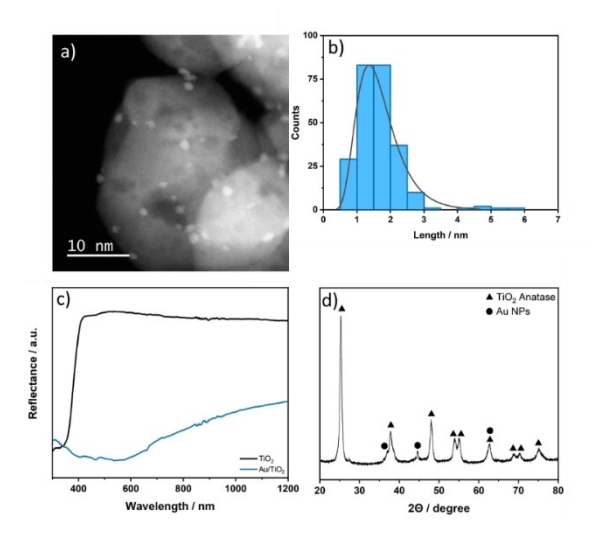


Figure 1. Characterization of the Au/TiO₂ catalyst. a) Representative HAADF-STEM image of the Au/TiO₂ catalyst showing the Au NPs on the TiO₂ support; b) Particle size distribution histogram; c) Diffuse reflectance UV–Vis-NIR spectra for TiO₂ (black curve) and Au/TiO₂ (blue curve); d) XRD pattern of the Au/TiO₂ nanocatalyst [TiO₂ 01-073-1764, Au 00-004-0784].

only achieved above the bandgap of TiO_2 in the UV region, while in the second case the absorption was broadened to the visible spectrum based on the LSPR of the Au nanoparticles. The powder X-ray diffraction (XRD) analysis confirmed the crystallinity of the anatase TiO_2 support, and displayed peaks at 38.2° , 44.4° and 64.5° of metallic Au (Figure 1d).

Sunlight powered continuous flow rWGS process

The CO₂ photoreduction experiments were performed in a tailored photoreactor system. The reactor was irradiated through a quartz window on top. N₂ was used as internal standard. The applied light source was a solar simulator (Newport Sol3A) equipped with an AM1.5 filter, with a tuneable light intensity up to 14 kW·m⁻² (=14 suns). To measure the catalyst bed temperature, a thermocouple placed in contact with the bottom of the catalyst bed (T_c) was used. A scheme of the system is provided in the ESI Figure S2. The reactor temperature was measured using a second thermocouple (T_r) . In the experiments under illumination, simulated sunlight was used as sole energy source without additional external heating of the reactor. Time zero was defined as the moment when the light was switched on. In line with our previous work on the rWGS batch process, we performed the continuous flow process at a pressure of 3.5 bar to ensure an overpressure in the reactor and prevent air from entering. In the thermocatalytic reference experiments (dark experiments), no light irradiation was used and the reactor was heated via electric heating rods. The reactant mixture was introduced after thermal equilibrium when the desired temperature was achieved, and this instance was considered time zero. This was done to avoid catalyst deactivation during the process of reactor heating. Since the rWGS reaction is limited by equilibrium and the temperature of

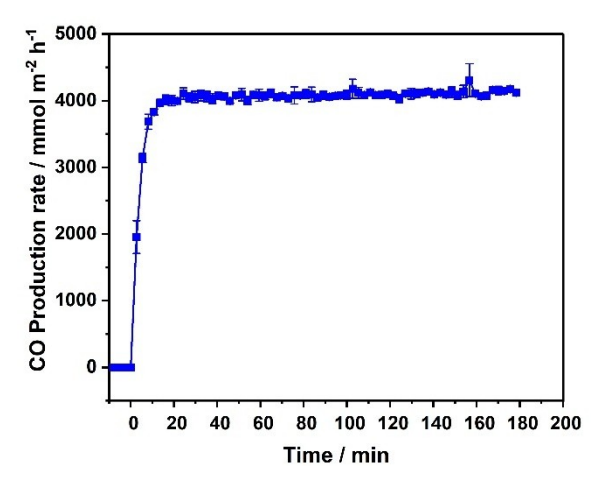


Figure 2. Average CO production rate with standard deviation as function of time. 75 mg Au/TiO₂ catalyst was loaded on the 3.14 cm² area designed for the catalyst bed holder using a 1:1 CO₂:H₂ ratio. Reaction conditions: 3.5 bar, total flow 135 mL·min⁻¹, 14.0 suns irradiation from solar simulator (1 sun = 1 kW·m⁻², AM1.5) without external heat.

the catalyst bed is rather low in our study (always below 200 °C), the CO₂ conversion is always below 5%. This ensures that we are not operating in a regime in which mass transfer is limiting the conversion rate. A continuous flow experiment under 14 suns irradiation without external heating was performed. This experiment was carried out *in triplo* to determine the experimental error. Using a CO₂:H₂ ratio of 1:1, the obtained CO production rate was $4086 \pm 57 \text{ mmol} \cdot \text{m}^{-2} \cdot \text{h}^{-1}$ and the apparent quantum efficiency (AQE) was 3.2% (ESI S3). The selectivity for CO was 96.9% (Figure 2) and only CH₄ was detected as a side product. During the 3 hours duration of the continuous flow experiment, both the activity and the selectivity of the reaction remained constant, and no catalyst deactivation was observed.

CO production rate: optimizing catalyst bed thickness

One of the main difficulties when comparing the performance of different plasmonic catalysts and results obtained by different labs is that there is not a standard protocol to test and report plasmon catalytic activities. Frequently, the catalytic activity is reported in mmol $g_{cat}^{-1} \cdot h^{-1}$. However, normalizing the production rate to the mass of the catalyst (or the mass of plasmonic metal) is not a useful normalization to compare different catalysts or results from different labs, because the reaction rate does not follow a linear increase with the photocatalyst mass due to the limited light penetration depth and corresponding shielding effect.^[16] It is therefore better to report the catalytic activity per m² illuminated area. To optimize the thickness of the catalyst bed, we studied the relationship between the CO production rate and the catalyst mass placed on the 3.14 cm² holder. Using 40 mg of catalyst, the illuminated surface area was completely covered. The CO production rate for the various loadings shows three different regimes with a distinct transition from regime 1 to regime 2 at 70 mg, and

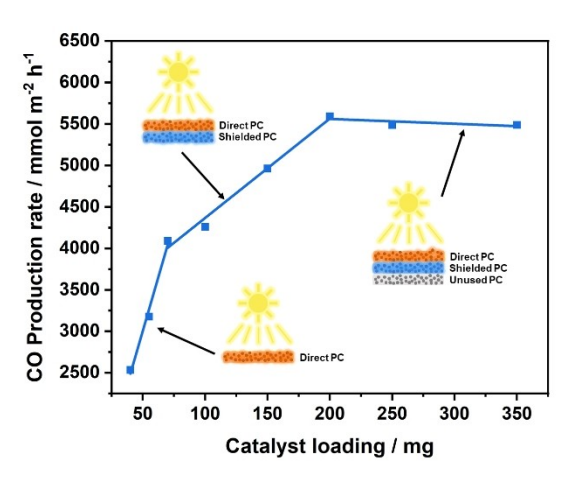


Figure 3. CO Production rate as function of catalyst loading on the 3.14 cm^2 holder designed for the Au/TiO₂ catalyst bed, and using a $1:1 \text{ CO}_2:H_2$ ratio. Reaction conditions: 3.5 bar, total flow $135 \text{ mL} \cdot \text{min}^{-1}$, 14.0 suns irradiation from solar simulator. (1 sun = $1 \text{ kW} \cdot \text{m}^{-2}$, AM1.5) without external heat.

from regime 2 to regime 3 at 200 mg loading (Figure 3). Up to 70 mg, all the catalyst material is directly exposed to light. We designated this regime as direct plasmon catalysis (DPC). At higher loadings - between 70 mg and 200 mg - the slope change indicates that part of the catalyst is not directly exposed to light because of shielding, but can nevertheless contribute to the catalytic process, e.g. via absorption of (scattered) light of a lower irradiance, or via transfer of heat from the photothermally heated top surface to the layer below (shielded PC). Above 200 mg, the CO production rate reaches a plateau, meaning that further addition of catalyst does not increase the CO production rate because it is neither illuminated nor heated (unused PC). Should be noticed, that as reported previously by our group, there is a temperature gradient present inside the illuminated catalyst bed, because of single-side illumination and poor thermal conductivity.[17a]

Photothermal vs. non-thermal contribution

To differentiate between photothermal and non-thermal contributors, the relationship between irradiance and the CO production rate was studied. When varying the irradiance, the rate of reactions solely initiated via a transfer of hot electrons to antibonding orbitals of adsorbed reactants displays a linear dependence on the irradiance, since the rate of the reaction is proportional to the photon flux. In contrast, photothermal reactions display an exponential relationship between the reaction rate and the irradiance, since the temperature of the catalyst is proportional to the light absorption and rate constants of chemical reactions typically follow an Arrheniustype of temperature dependence. As shown in Figure 4, the CO production rate increases exponentially when the light intensity is raised from 6 to 14 suns. However, the catalyst bed temperature increases linearly from 78°C to 152°C as can be

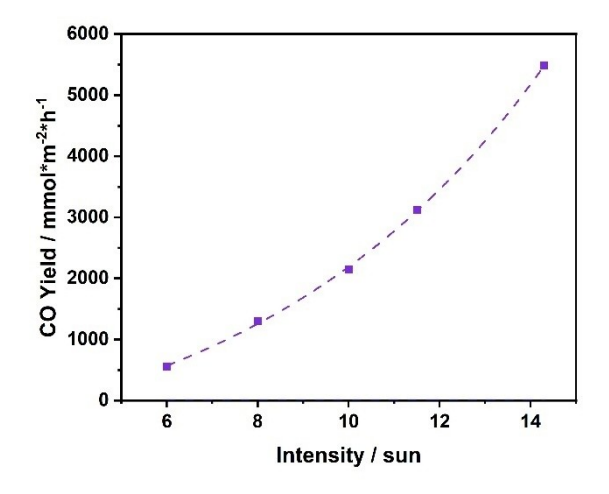


Figure 4. CO Production rate as function of irradiance. Reaction conditions: 200 mg Au/ TiO_2 , 1:1 CO₂:H₂ ratio, 3.5 bar, total flow 135 mL·min⁻¹ without external heat.

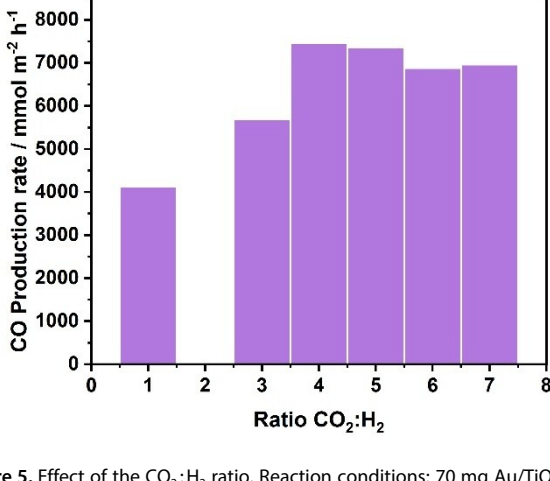


Figure 5. Effect of the CO₂: H_2 ratio. Reaction conditions: 70 mg Au/TiO₂, 3.5 bar, total flow 135 mL·min⁻¹, 14.0 sun irradiation from solar simulator. (1 sun = 1 kW*m⁻², AM1.5), without external heat.

observed in Figure SI4 in the ESI. There is a temperature gradient present inside the illuminated catalyst bed, because of single-side illumination and poor thermal conductivity. For a more accurate determination of E_A , the temperature at various depths inside the catalyst bed should be monitored *in operando*, for which no technology is available to date. The observed exponential relationship demonstrates that the main contributor to this process is photothermal heating, but does not exclude an additional photochemical contributor. In a previous study, we have concluded that Au NPs are mainly responsible for the light absorption and the promotion of the reaction, since UV light above the bandgap of TiO_2 had no significant influence on the process.

Effect of the CO2: H2 ratio

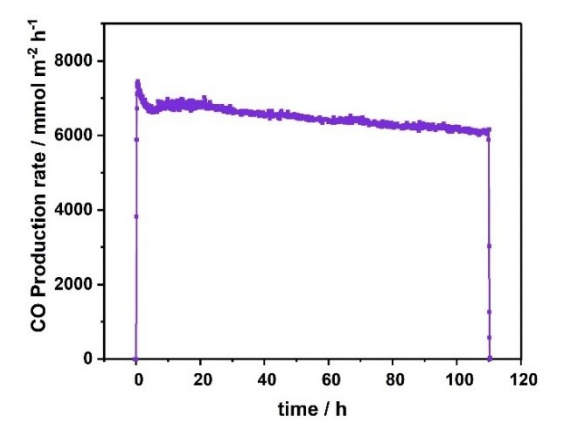
The dependence of the CO production rate on the CO₂:H₂ ratio was studied for 6 different feedstock compositions (ESI S5) from the stochiometric ratio (1:1) to CO_2 excess of (7:1). The total flow rate was kept constant as we varied the CO₂ share in the starting gas mixture from 44.4% for the ratio (1:1) to 77.8% for the ratio (7:1), whilst keeping the N_2 share constant at 11.1% (ESI table S5). The CO production rate shows an increase when increasing the CO₂:H₂ ratio (Figure 5) until reaching a maximum at CO₂:H₂ ratio of 4:1-5:1, achieving a CO production rate of 7423 mmol \cdot m $^{-2} \cdot$ h $^{-1}$ which corresponds to an AQE of 4.15%. At higher ratios, the CO production rate slightly decreases. The CO selectivity remained constant between the different reactant ratios, and was always higher than 96%. An important contributor to the increase in reaction rate with increasing CO₂:H₂ ratio is the increase in catalyst bed temperature. The catalyst bed temperature increases linearly with increasing CO_2 : H_2 ratio from 134 °C (ratio of 1:1) to 141.5 °C (ratio of 7:1) (ESI Figure SI5). This can be attributed to the lower thermal conductivity of CO₂ when compared to H₂. The catalyst surface temperature should be much higher, and this temperature should be monitored *in operando*, for which no technology is available to date.

Thermocatalytic experiments (dark experiments) were performed as reference experiments to compare the catalytic activity and selectivity to the experiments under light. The reactor was heated from the laterals using electrical heating rods. The system reached the desired temperature under N₂ flow and was then filled with the reactants in order to avoid catalyst deactivation during the heating process. The CO production rate was studied from 140 °C to 200 °C using a 4:1 CO₂:H₂ ratio, 70 mg of Au/TiO₂ catalyst, 3.5 bar pressure and a total flow of 135 mL·min⁻¹ (See Figure S6 in the ESI). The CO production rate increases exponentially with rising temperature. The CO production rate achieved in dark at 200°C was 3716 mmol⋅m^{-2⋅}h⁻¹ at CO selectivity of 80%, with CH₄ as sole side product. The activity and selectivity are significantly lower when compared to the illuminated counterpart, viz. 3716 mmol·m^{-2·}h⁻¹ (dark, 200 °C) vs. 7423 mmol·m⁻²·h⁻¹ (light, 14 suns) and 80% (dark, 200°C) vs. 96% (light, 14 suns), respectively. We propose that the difference in selectivity could be caused by the promotion of H₂O and CO desorption through charge transfer of plasmon generated charges, limiting further reduction to CH₄.

Catalyst stability

The catalyst stability in the continuous flow sunlight powered rWGS process was studied for 110 h. The first 24 h showed a production decrease until reaching 90% of the initial CO production (Figure 6a). After 110 h we still observed more than 82% of the initial CO production without displaying any abrupt deactivation. The minor gradual deactivation may be attributed to H₂O accumulation in the photoreactor, since the reactor itself remains at room temperature. The spent catalyst was characterized to investigate whether morphology changes occurred during the reaction. As determined by HAADF-STEM analyses,





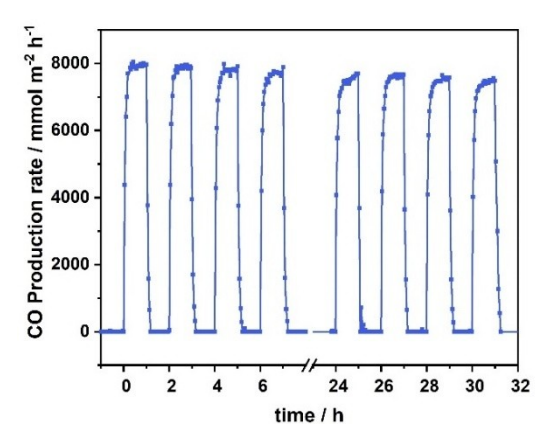


Figure 6. Catalyst stability test. a) CO production rate as function of time, b) on-off test where the solar simulator was turned on/off every hour. Reaction conditions: 70 mg Au/TiO $_2$, 4:1 CO $_2$:H $_2$ ratio, 3.5 bar, total flow 135 mL·min $^{-1}$, 14.0 sun irradiation from solar simulator. (1 sun = 1 kW*m $^{-2}$, AM1.5) without external heat.

the average Au particle size was 1.82 nm following a lognormal distribution (ESI S7, Figure S7a–b). This Au nanoparticle size does not significantly deviate from the initial value of 1.70 nm. This indicates a good structure stability during the 110 h experiment with no signs of catalyst sintering.

The high selectivity of the catalyst could be attributed to promotion of CO desorption through charge transfer of plasmon generated charges, as suggested in previous studies. [7e,11,18] In dark reference experiments, the selectivity is substantially lower due to further hydrogenation of adsorbed CO to CH₄. The difference in activity between the light-powered and thermal rWGS reaction may be caused by the difference in surface temperature of the illuminated catalyst bed and the temperature measured by the thermocouple in contact with the bottom of the catalyst bed. As shown in a previous study, this difference may be of the order of 150 °C. [17a] The high stability of the catalyst is related to the rather low operating temperature.

Since solar irradiation fluctuates over time, the CO production rate and the catalyst stability was further investigated by performing on/off experiments. Stopping and starting the process can have a substantial impact on the catalytic performance. Light was switched on during 1 h, switched off for one

hour, for 4 consecutive cycles. Afterwards, the reactor was off overnight and the next day 4 extra cycles were performed. After 4 cycles, the CO production rate was similar to the first cycle (98%, 7888 mmol·m $^{-2}\cdot h^{-1}$). After the 4th cycle the catalyst remained at RT in dark overnight (17 h). The next day in the 5th cycle we achieved 96% of the starting production rate (7694 mmol·m $^{-2}\cdot h^{-1}$) after 1 h under illumination. The initial CO production rate was lower, most probably due to the remained adsorbed water on the catalyst bed. The 8th cycle had a production rate of 7567 mmol·m $^{-2}\cdot h^{-1}$ that corresponded to 94% of the CO production rate obtained in the first cycle.

Conclusions

In conclusion, the present study shows that plasmonic Au/TiO₂ nanocatalysts are efficient in the rWGS process using sunlight as sole and sustainable energy source. To scale up and progress towards an industrially applicable technology, we successfully transferred from a batch to a continuous flow process. Furthermore, we studied the effect of the catalyst layer thickness on the CO production rate, and three regimes were identified as DPC, SPC and UPC. The results are applied to maximize the CO production rate per m² illuminated catalyst bed to minimize land use. Under optimized conditions, we achieved a CO production rate of 7423 mmol·m⁻²·h⁻¹ and a selectivity of 96%, which corresponded to an AQE of 4.15%. Both activity and selectivity were significantly higher for the sunlight-powered process when compared to thermal reference experiments in dark, viz. 3716 mmol·m^{-2·}h⁻¹ (dark, 200 °C) vs. 74230 mmol·m⁻²·h⁻¹ (light, 14 suns) and 80% (dark, 200 °C) vs. 96% (light, 14 suns), respectively. Furthermore, we demonstrated that the catalyst was stable, both over a prolonged period of time (82% activity remained after 110 h) and in on-off experiments to mimic discontinuous sunlight powered production (94% activity remained after 8 cycles).

Experimental

Synthesis of the Au/TiO₂ catalyst. The Au/TiO₂ catalyst was synthesized by a deposition-precipitation method, based on previously reported methodologies. [19] HAuCl₄ 3H₂O (Sigma Aldrich, 99.9%) was used as the Au precursor. The Au precursor (200 mg) was added to ultra-filtered water (Milli-Q Millipore, 18.2 M Ω cm, 100 mL) in vigorous stirring. Then, the pH of the solution was adjusted to 9 by adding NaOH (0.1 M). Once the pH stabilized, TiO₂ (1.00 g, 99.5% anatase, loLiTec Nanomaterials) was added to the mixture, followed by an adjustment of the pH back to 9. The dispersion was left in vigorous stirring for 48 hours at room temperature, keeping a continuous control of the pH with a pH meter. The solid was recuperated by filtration and extensively washed with ultra-filtered water (Milli-Q Millipore, 18.2 M Ω cm). Subsequently, the solid was dried in a vacuum oven at 100°C for 2 hours and calcinated in a tube furnace at 200 °C in a 20:80 O₂:Ar atmosphere for 4 h, following a heating ramp of 2°C⋅min⁻¹. For this whole study, 10 syntheses of 1 g were done and their products were mixed to reduce the influence of batch-to-batch variations on the photocatalytic tests. The characterization shown corresponds to the obtained mixture.





Photocatalytic tests: The sunlight-powered CO₂ hydrogenation tests were performed in a custom-made flow photoreactor, equipped with a quartz window at the top to allow the light irradiation. The solar simulator (Newport Sol3A) was placed above it and was equipped with a high flux beam concentrator (Newport 81030), and AM1.5 filter and the possibility to introduce cut-off filters. The irradiated area was about 3.14 cm² and was covered by the sample. The reactor has three thermocouples to measure the temperatures at the top and bottom of the reactor, and under the catalyst bed. A schematic representation of the reactor setup can be seen in ESI Figure S2. In a typical run, 70 mg of the catalyst was put in the reactor, after removing the air with three times with N₂ and vacuum purge cycles, the reactor was filled with a mixture of H_2 (Linde 6.0), CO_2 (Linde 4.5) and N_2 (Linde 5.0), with a H_2 : CO_2 : N_2 flow of 24:96:15 mLmin⁻¹, with the pressure regulated at 1.85 using a back pressure controller. The time 0 is considered when light was switched on. For dark experiments, the reactor was heated up until the desired temperature under nitrogen flow, and when the temperature was stable the CO₂ and H₂ were introduced. The products were analyzed by a gas chromatograph (Compact GC, Global Analyzer Solutions), which was directly coupled to the output of the reactor. The GC was equipped with three channels, two microthermal conductivity detectors (TCD) and one flame ionization detector (FID). The peak areas were used to determine the ratio of each compound based on calibration, using N₂ as an internal standard. If products were present in the time zero analysis, this value was subtracted from the measurements in the following

Acknowledgements

P. M. M., J. R., K. W. B., N. M., P. B., and F. S. acknowledge the financial support from the European Fund for Regional Development through the cross-border collaborative Interreg V program Flanders, the Netherlands (project LUMEN), co-financed by the Belgian province of Limburg and the Dutch provinces of Limburg and Noord-Brabant. M.A.V. acknowledges Solliance and the Dutch province of Noord-Brabant for funding the TEM facility. We thank Prof. Dr. Wouter Marchal from Hasselt University for the ICP analyses.

Conflict of Interests

There are no conflicts to declare.

Data Availability Statement

The data that support the findings of this study are available from the corresponding author upon reasonable request.

Keywords: Carbon dioxide \cdot photochemistry \cdot reverse Water gas Shift flow \cdot solar light \cdot surface plasmon resonance

- [1] N. von der Assen, L. J. Müller, A. Steingrube, P. Voll, A. Bardow, *Environ. Sci. Technol.* **2016**, *50*, 1093–1101.
- [2] a) S. Hernández, M. Amin Farkhondehfal, F. Sastre, M. Makkee, G. Saracco, N. Russo, Green Chem. 2017, 19, 2326–2346; b) A. Senocrate, C.

- Battaglia, J. Energy Storage 2021, 36, 102373; c) A. E. Nogueira, G. T. S. T. Silva, J. A. Oliveira, O. F. Lopes, J. A. Torres, M. Carmo, C. Ribeiro, ACS Appl. Energ. Mater. 2020, 3, 7629–7636; d) F. Sastre, M. J. Muñoz-Batista, A. Kubacka, M. Fernández-García, W. A. Smith, F. Kapteijn, M. Makkee, J. Gascon, ChemElectroChem 2016, 3, 1497–1502; e) E. Pérez-Gallent, S. Turk, R. Latsuzbaia, R. Bhardwaj, A. Anastasopol, F. Sastre-Calabuig, A. C. García, E. Giling, E. Goetheer, Ind. Eng. Chem. Res. 2019, 58, 6195–6202.
- [3] a) S. Remiro-Buenamañana, H. García, ChemCatChem 2018, 11, 342–356;
 b) A. Corma, H. García, J. Catal. 2013, 308, 168–175;
 c) D. Rodriguez-Padron, R. Luque, M. J. Munoz-Batista, Top Curr Chem (Cham) 2019, 378, 3
- [4] a) X. Meng, L. Liu, S. Ouyang, H. Xu, D. Wang, N. Zhao, J. Ye, Adv. Mater. 2016, 28, 6781–6803; b) H.-H. Shin, J.-J. Koo, K. S. Lee, Z. H. Kim, Applied Materials Today 2019, 16, 112–119; c) X. Zhang, Y. L. Chen, R. S. Liu, D. P. Tsai, Rep. Prog. Phys. 2013, 76, 1–13; d) R. Long, Y. Li, L. Song, Y. Xiong, Small 2015, 11, 3873–3889; e) X. Ren, E. Cao, W. Lin, Y. Song, W. Liang, J. Wang, RSC Adv. 2017, 7, 31189–31203; f) S. Li, P. Miao, Y. Zhang, J. W. B. Zhang, Y. Du, X. Han, J. Sun, P. Xu, Adv. Mater. 2020, 33, e2000086, https://doi.org/10.1002/adma.202000086; g) Y. Zhao, W. Gao, S. Li, G. R. Williams, A. H. Mahadi, D. Ma, Joule 2019, 3, 920–937.
- [5] a) K. Sytwu, M. Vadai, J. A. Dionne, Adv. Phys. 2019, 4, 398–422; b) E. Kazuma, Y. Kim, Angew. Chem. Int. Ed. Engl. 2019, 58, 4800–4808.
- [6] a) G. Baffou, R. Quidant, Chem. Soc. Rev. 2014, 43, 3898–3907; b) J. C. Scaiano, K. Stamplecoskie, J. Phys. Chem. Lett. 2013, 4, 1177–1187.
- [7] a) F. Sastre, A. V. Puga, L. Liu, A. Corma, H. García, JACS 2014, 136, 6798–6801; b) C. Choe, B. Lee, A. Kim, S. Cheon, H. Lim, Green Chem. 2021, 23, 9502–9514; c) U. Ulmer, T. Dingle, P. N. Duchesne, R. H. Morris, A. Tavasoli, T. Wood, G. A. Ozin, Nat. Commun. 2019, 10, 3169; d) F. Sastre, C. Versluis, N. Meulendijks, J. Rodríguez-Fernández, J. Sweelssen, K. Elen, M. K. Van Bael, T. den Hartog, M. A. Verheijen, P. Buskens, ACS Omega 2019, 4, 7369–7377; e) P. Martínez Molina, N. Meulendijks, M. Xu, M. A. Verheijen, T. Hartog, P. Buskens, F. Sastre, ChemCatChem 2021, 13, 4507–4513; f) J. Volders, K. Elen, A. Raes, R. Ninakanti, A. S. Kelchtermans, F. Sastre, A. Hardy, P. Cool, S. W. Verbruggen, P. Buskens, M. K. Van Bael, Nanomaterials (Basel) 2022, 12, 4153; g) B. van der Zwaan, R. Detz, N. Meulendijks, P. Buskens, Fuel 2021, 311, 122547; h) J. Rohlfs, K. W. Bossers, N. Meulendijks, F. Valega Mackenzie, M. Xu, M. A. Verheijen, P. Buskens, F. Sastre, Catalysts 2022, 12, 126.
- [8] a) J.-P. Lange, Catal. Today 2001, 64, 3-8; b) Y. Wang, Q. Xia, Chem 2018,
 4, 2741-2743; c) A. Yahyazadeh, A. K. Dalai, W. Ma, L. Zhang, Reactions 2021, 2, 227-257; d) S. Li, S. Haussener, Appl. Energy 2023, 334, 120617.
- [9] D. U. Nielsen, X.-M. Hu, K. Daasbjerg, T. Skrydstrup, Nature Catalysis 2018, 1, 244–254.
- [10] X. Su, X. Yang, B. Zhao, Y. Huang, J. Energy Chem. 2017, 26, 854–867.
- [11] A. A. Upadhye, I. Ro, X. Zeng, H. J. Kim, I. Tejedor, M. A. Anderson, J. A. Dumesic, G. W. Huber, Catal. Sci. Technol. 2015, 5, 2590–2601.
- [12] a) B. Tahir, M. Tahir, N. A. S. Amin, Clean Technol. Environ. Policy 2016, 18, 2147–2160; b) M. Tahir, B. Tahir, N. A. S. Amin, Z. Y. Zakaria, J. CO2 Util. 2017, 18, 250–260; c) M. Tahir, B. Tahir, N. A. S. Amin, Appl. Catal. A 2017, 204, 548–560.
- [13] L. F. Bobadilla, J. L. Santos, S. Ivanova, J. A. Odriozola, A. Urakawa, ACS Catal. 2018, 8, 7455–7467.
- [14] a) M. Tahir, B. Tahir, Appl. Surf. Sci. 2016, 377, 244–252; b) P. López-Caballero, A. W. Hauser, M. Pilar de Lara-Castells, J. Phys. Chem. C 2019, 123, 23064–23074; c) C. Kim, S. Hyeon, J. Lee, W. D. Kim, D. C. Lee, J. Kim, H. Lee, Nat. Commun. 2018, 9, 3027; d) H. Robatjazi, H. Zhao, D. F. Swearer, N. J. Hogan, L. Zhou, A. Alabastri, M. J. McClain, P. Nordlander, N. J. Halas, Nat. Commun. 2017, 8, 27; e) L. Wan, Q. Zhou, X. Wang, T. E. Wood, L. Wang, P. N. Duchesne, J. Guo, X. Yan, M. Xia, Y. F. Li, A. A. Jelle, U. Ulmer, J. Jia, T. Li, W. Sun, G. A. Ozin, Nature Catalysis 2019, 2, 889–898.
- [15] a) D. Mateo, D. De Masi, J. Albero, L. M. Lacroix, P. F. Fazzini, B. Chaudret, H. Garcia, Chemistry 2018, 24, 18436–18443; b) D. Mateo, J. Albero, H. García, Joule 2019, 3, 1949–1962; c) X. Yan, W. Sun, L. Fan, P. N. Duchesne, W. Wang, C. Kubel, D. Wang, S. G. H. Kumar, Y. F. Li, A. Tavasoli, T. E. Wood, D. L. H. Hung, L. Wan, L. Wang, R. Song, J. Guo, I. Gourevich, A. A. Jelle, J. Lu, R. Li, B. D. Hatton, G. A. Ozin, Nat. Commun. 2019, 10, 2608; d) R. Grote, R. Habets, J. Rohlfs, F. Sastre, N. Meulendijks, M. Xu, M. Verheijen, K. Elen, A. Hardy, M. van Bael, T. den Hartog, P. Buskens, ChemCatChem 2020, 12, 5618–5622; e) X. Meng, T. Wang, L. Liu, S. Ouyang, P. Li, H. Hu, T. Kako, H. Iwai, A. Tanaka, J. Ye, Angew. Chem. 2014, 126, 11662–11666; f) D. Burova, J. Rohlfs, F. Sastre, P. M. Molina, N. Meulendijks, M. A. Verheijen, A.-S. Kelchtermans, K. Elen, A. Hardy, M. K. Van Bael, P. Buskens, Catalysts 2022, 12, 284; g) F. Sastre, A. Corma, H. García, Angew. Chem. Int. Ed. 2013, 52, 12983–12987; h) J.





- Albero, E. Dominguez, A. Corma, H. García, Sustain. Energy Fuels 2017, 1, 1303–1307
- [16] a) M. Qureshi, K. Takanabe, Chem. Mater. 2016, 29, 158–167; b) N. Serpone, J. Photochem. Photobiol. A 1997, 104, 1–12; c) Z. Wang, T. Hisatomi, R. Li, K. Sayama, G. Liu, K. Domen, C. Li, L. Wang, Joule 2021, 5, 344–359; d) H. Kisch, Angew. Chem. Int. Ed. Engl. 2010, 49, 9590–9581.
- [17] a) M. Xu, T. den Hartog, L. Cheng, M. Wolfs, R. Habets, J. Rohlfs, J. van den Ham, N. Meulendijks, F. Sastre, P. Buskens, *ChemPhotoChem* 2022, 6 (4), 6; b) G. Baffou, P. Berto, E. Bermudez Urena, R. Quidant, S. Monneret, J. Polleux, H. Rigneault, *ACS Nano* 2013, 7, 6478–6488; c) I.-W. Un, Y. Sivan, "Photothermal effects in plasmonic assisted photocatalysis: a parametric study", Proc. SPIE 11694, Photonic and Phononic Properties of Engineered Nanostructures XI, 116940D (5 March 2021); https://doi.org/10.1117/12.2582733; d) Y. Dubi, I. W. Un, Y. Sivan, *Chem. Sci.* 2020, *11*, 5017–5027.
- [18] X. Zhang, X. Li, D. Zhang, N. Q. Su, W. Yang, H. O. Everitt, J. Liu, Nat. Commun. 2017, 8, 14542.
- [19] a) R. Zanella, S. Giorgio, C. R. Henry, C. Louis, J. Phys. Chem. B 2002, 106, 7634–7642; b) J. Matos, T. Marino, R. Molinari, H. García, Appl. Catal. A 2012, 417 (418), 263–272.

Manuscript received: May 8, 2023 Revised manuscript received: May 22, 2023 Accepted manuscript online: May 30, 2023 Version of record online: June 5, 2023